Table 2
Beam property of CBNS under free-air condition compared with KUR epithermal mode.

	Epi-thermal neutron flux (Φ_{epi}) (n/cm^2/s)	Fast-neutron dose/Φ_{epi} (Gy/n cm^2)	Gamma-ray dose/ Φ_{epi} (Gy/n cm^2)
KUR (epi-thermal)	7.30E+08	9.10E−13	2.40E−13
Accelerator	1.88E+09	5.84E−13	7.75E−14

heavy-water thickness in the spectrum shifter and by opening and closing of the cadmium and boral thermal neutron filters. BNCT using epithermal-neutron irradiation was started in earnest in December 2001 at HWNIF. As of March 2006, 189 BNCT treatments using epithermal-neutron incidence were carried out: 82 for brain tumors, 93 for recurrent head and neck tumors, and 14 for body tumors.

2.3. Beam properties

Fig. 6 shows the neutron spectrum evaluated at the surface of gamma-ray shielding. In this calculation, the collimator was removed because of the free-air condition. The spectrum of KUR is also plotted in Fig. 6. This epithermal-neutron spectrum formed by using a cadmium thermal neutron filter of KUR is most-often used in BNCT treatment.

The accelerator-based neutron spectrum has a peak in the energy range of 10–20 keV. In the case of this spectrum, the definition of the energy range of epithermal is from 0.5 eV to 40 keV, because as mentioned above (Section 2.1.3), this region is most effective for the treatment of deep tumors. In this article, the energy region below 0.5 eV is defined as the thermal region; that above 40 keV, as the fast-neutron region. In comparison with KUR, CBNS has the potential of better treatment effectiveness because of a better energy spectrum.

Table 2 shows the contamination of absorbed dose by fast-neutron and gamma-ray components under the free-air condition. Each absorbed dose was derived from the neutron flux at the position of the gamma-ray shield and the conversion factor to the absorbed dose published in ICRP-74 [12]. The human component was assumed to be H: 11.1, C: 12.6, N: 2.0 and O: 74.3 (wt%). It is confirmed that with regard to the contaminations caused by fast neutrons and gamma rays, CBNS is superior to KUR. The epithermal-neutron flux of CBNS was larger than that of KUR by a factor of 2.5.

In order to confirm the beam flatness, the neutron flux was evaluated at the collimator surface with the collimator aperture of ϕ25 cm. Fig. 7 shows the relationship between flux distribution of thermal-, epithermal- and fast-neutrons and the distance from beam axis. As compared with its value at the beam axis, the epithermal-neutron flux at a distance of 5 cm from the beam axis and at the collimator edge reduced by 10% and 30%, respectively. Because neutrons pass through a material with some scattering reaction with it, reducing their energy, the treatment beam contained neutrons having several directions. However, in actual treatment, the patient is positioned directly in front of the collimator and neutrons that are injected into the patient's body diffuse. Therefore, to use our treatment beam compared with completely flat beam has a little influence in treatment effectiveness.

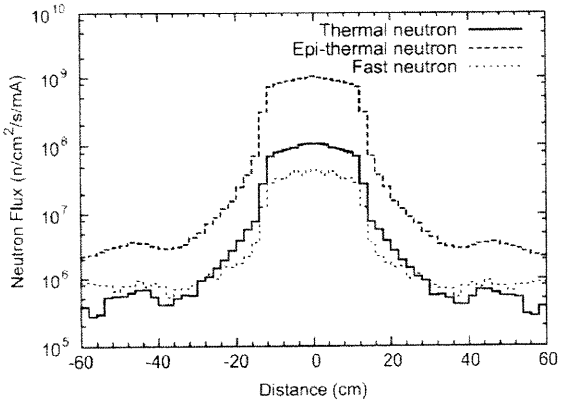

Fig. 7. Flux distribution of thermal, epithermal and fast neutrons as a function of distance from beam axis.

The thermal-, epithermal- and fast-neutron flux decreased at locations far from the beam axis. At a distance of 40 cm from the beam axis, each flux attenuated by two orders of magnitude. It is confirmed that the absorbed dose also reduced at this distance.

3. Results and discussion

3.1. Comparison of beam characteristics in phantom

At KURRI, BNCT clinical trials have been performed using epithermal neutrons. In order to evaluate the dose distribution in a patient's body, the treatment planning system of SERA (Simulation Environment for Radiotherapy Applications) [13,14] was used. For evaluating the properties of CBNS, the experience of past clinical trials using SERA in KUR is referred. In terms of the distribution of thermal-neutron flux in a phantom, it is revealed that the experimental data agree well with the calculated data of SERA within an error of 3% [15].

SERA can make a voxel model for three-dimensional neutron transport calculation using CT/MRI images and output the neutron flux and gamma-ray flux at each voxel. The absorbed dose is derived from the multiplication between the conversion factor served by SERA and the neutron and gamma-ray flux at each voxel.

The main absorbed dose in BNCT consists of the boron dose by the $^{10}B(n,\alpha)^7Li$ reaction, the nitrogen dose by the $^{14}N(n,p)^{14}C$, the hydrogen dose by the $^1H(n,n')^1H$, the gamma dose in patient's body by the $^1H(n,\gamma)^2H$, and the gamma dose produced by the components of BSA and collimator.

The source information for CBNS of SERA, such as neutron and gamma-ray spectrum and angular distribution, is derived from the calculation output of MCNPX. The source information of KUR is epithermal-neutron mode, which is used for actual treatment in KUR. As the parameter for evaluation of epithermal neutron sources, therapeutic time and advantage depth (AD) and advantage depth at 30 Gy-eq (AD30) are used.

AD is the depth in the phantom for a tumor dose distribution of 10 Gy-eq, when the peak of the normal brain dose is 10 Gy-eq. It corresponds to a larger dose that is prescribed for a deep tumor.

We selected the value of 10 Gy-Eq as maximum allowed dose in order to limit the cumulative dose to normal brain tissue lower than 100 Gy. Mayer et al. showed that radiation-induced normal brain tissue necrosis was found to occur at larger than 100 Gy [16]. In our facility, the BNCT treatments were adapted for recurrent brain tumors that were already treated by the conventional radiotherapy up to 60–70 Gy in 2-Gy fractions. To evaluate the cumulative dose to normal brain tissue after BNCT treatment, assuming an α/β coefficient of 3 for normal brain tissue, according to the linear-quadratic model, in single-fractionated BNCT, a 10 Gy-Eq single dose would equal radiation doses of 26 Gy in 2-Gy fractions [17]. Total cumulative dose to normal brain tissue is sufficiently lower than 100 Gy.

On the other hand, Laramore et al. showed a tumor dose-response curve for BNCT. They noted that approximately 30 Gy-Eq

must be given to the tumor [18]. Thus, we defined AD30 for tumor dose. The dose distribution in the phantom is compared between CBNS and KUR. Fig. 8 shows a schematic layout of the irradiation in BNCT for a brain tumor.

In the treatment by BNCT, before and during neutron irradiation, the ^{10}B-loaded medicine (in this article, Borono-phenyl-alanine: BPA is assumed), which preferentially accumulates in tumor cells compared with normal cells, is infused. The prescribed dose is determined by the difference of accumulation between tumor and normal (T/N ratio) cells and the boron concentration in the blood of a patient. The accumulation of BPA is detected by using the PET analysis with the BPA labeled by ^{18}F nuclei. Whether the treatment case is adopted for BNCT or not, the T/N ratio is derived from PET analysis. In the KURRI protocol, the case with a T/N ratio of larger than 2.5 is adopted for BNCT.

The relative biological effectivenesses (RBEs) for nitrogen, hydrogen and gamma rays are 3.0, 3.0 and 1.0, respectively. The compound biological effectivenesses (CBEs) for tumor and normal brain are 3.8 and 1.35, respectively. For evaluating effectiveness of treatment, the T/N ratios of 2.5, 3.5 and 4.5 were selected. The therapeutic time is determined by the dose limit for the normal brain of 10 Gy-eq.

Fig. 9 shows the distribution of biological effect weighted dose in the phantom as a function of the phantom depth. The boron concentration is assumed to be 24 ppm. In the condition of all T/N ratios, the RBE dose distribution of KUR is better than that of CBNS until a depth of 4 cm. On the other hand, at a position deeper than 4 cm, the accelerator exhibits better properties than KUR.

Figs. 10–12 show AD, AD30, and the therapeutic time as a function of the boron concentration in blood. In the case of the T/N ratios of 2.5, 3.5 and 4.5, AD of the accelerator is larger than that of KUR. For every boron concentration, CBNS can prescribe the dose at a 5–6% deeper tumor position compared with KUR.

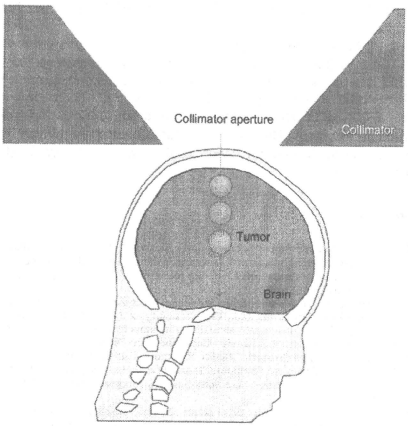

Fig. 8. Schematic image of the irradiation of brain tumor using head phantom.

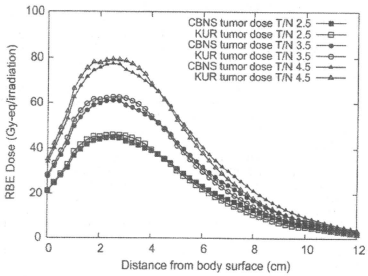

Fig. 9. Relationship between the biological effect weighted dose and the depth in head phantom.

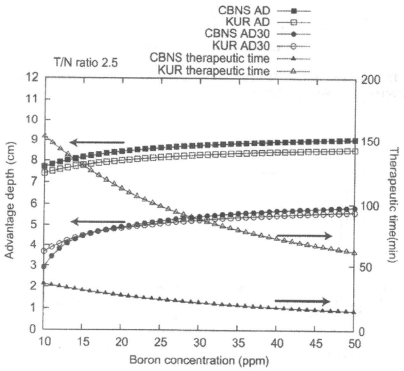

Fig. 10. Relationship of AD, AD30 Gy-eq and therapeutic time as a function of boron concentration in blood for T/N ratio of 2.5.

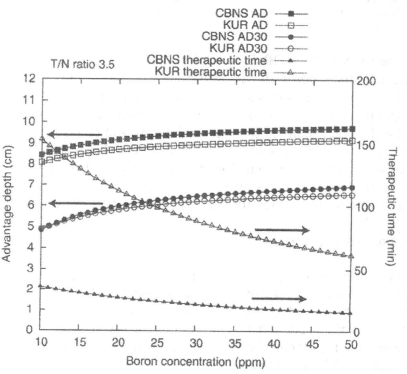

Fig. 11. Relationship of AD, AD30 Gy-eq and therapeutic time as a function of boron concentration in blood for T/N ratio of 3.5.

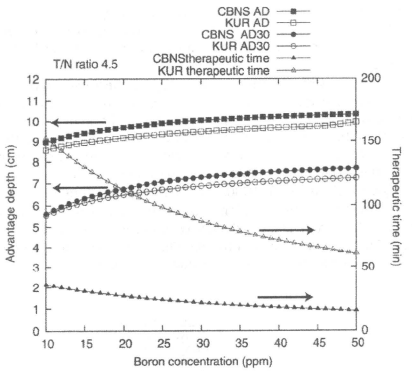

Fig. 12. Relationship of AD, AD30 Gy-eq and therapeutic time as a function of boron concentration in blood for T/N ratio of 4.5.

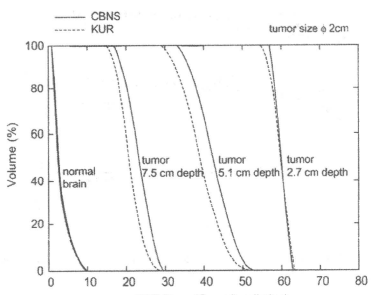

Fig. 13. Dose-volume histograms for the tumors, located at 2.7, 5.1 and 7.5 cm depth distance from head surface, and normal brain.

The superiority of CBNS for AD30 is indicated by the larger T/N ratio and higher boron concentration. For example, AD30s of CBNS at the boron concentrations of 12, 24 and 36 ppm and the T/N ratio of 3.5 are increased by 0.5%, 3.4% and 4.5% compared with KUR.

On the other hand, in the case of the T/N ratio of 2.5 shown in Fig. 10, AD30 of KUR is larger than that of CBNS with the boron of concentration of 15 ppm. This result is caused by the opposite dose distribution at a shallower depth in the phantom. The therapeutic time of the accelerator is one-quarter of that of KUR.

3.2. Dose-volume histogram analysis

Dose-volume histogram (DVH) analysis is performed for the actual treatment to evaluate the beam properties. The irradiation condition shown in Fig. 8 of the 2-cm-diameter tumors located at the depths of 2.7, 5.1 and 7.5 cm is assumed. The collimator aperture diameter is 10 cm; the boron concentration and T/N ratio are 24 ppm and 3.5, respectively.

The mean normal brain doses for KUR and the accelerator, when the maximum dose is 10 Gy-eq, are 2.5 and 2.6 Gy-eq, respectively. In Fig. 13, the dose distribution of normal brain revealed by DVH for KUR is similar to that for the accelerator. For the tumor located at the depth of 2.7 cm, the tumor dose distributions for KUR and the accelerator almost overlap. The mean tumor dose of the accelerator for the tumors located at the depths of 5.1 cm and 7.5 cm are, respectively 10% and 18% larger than those of KUR. These results also indicated the effectiveness of the accelerator for treating deeply situated tumors using the DVH analysis.

4. Conclusion

BSA is optimized for Be targets and cyclotron-based epithemal-neutron sources by Monte Carlo simulation. With regard to the dose contamination caused by the fast neutrons and gamma rays present in the treatment beam, CBNS is superior to the present KUR facility. The evaluation of the dose distribution in a phantom revealed that AD and AD30 of CBNS with the boron concentration of 10–50 ppm and the T/N ratios of 2.5, 3.5 and 4.5 are superior to those of KUR, except for the following conditions of AD30. AD30 of KUR under the limited conditions such as a boron concentration of less than 15 ppm and the T/N ratio of 2.5 is better that of CBNS.

At KURRI, we aim to establish CBNS, which is now under construction, by 2009. KUR also will restart in the middle of 2009. KURRI has the ractor- and accelerator-based neutron sources for BNCT. KURRI is the unique facility in the world. The treatment using CBNS will be performed on the basis of the optimization presented in this article. The accelerator-based neutron source can be located near the hospital; this work could lead to the future development of BNCT.

References

[1] Minoru Suzuki, Yoshinori Sakurai, Satoru Hagiwara, Shinichiro Masunaga, Yuko Kinashi, Kenji Nagata, Akira Maruhashi, Koji Ono, First attempt of boron neutron capture therapy (BNCT) for hepatocellular carcinoma, Jpn. J. Clin. Oncol. 37 (5) (2007) 376.
[2] Minoru Suzuki, Yoshinori Sakurai, Shinichiro Masunaga, Yuko Kinashi, Kenji Nagata, Akira Maruhashi, Koji Ono, Feasibility of boron neutron capture therapy (BNCT) for malignant pleural mesothelioma from a viewpoint of dose distribution analysis, Int. J. Radiat. Oncol. Biol. Phys. 66 (5) (2006) 1584.
[3] Shunshke Yonai, Takao Aoki, Takashi Nakamura, Hiroshi Yashima, Mamoru Baba, Hitoshi Yokobori, Yoshihisa Tahara, Feasibility study on epithermal neutron field for cyclotron-based boron neutron capture therapy, Med. Phys. 30 (8) (2003) 2021.
[4] Yoshihisa Tahara, Yasushi Oda, Takako Shiraki, Takehiko Tsutsui, Hitoshi Yokobori, Shunsuke Yonai, Mamoru Baba, Takashi Nakamura, Engineering design of a spallation reaction-based neutron generator for boron neutron capture therapy, J. Nucl. Sci. Technol. 43 (1) (2006) 9.
[5] MCNPX User's Manual Version 2.4.0, LA-CP-02-408, Los Alamos National Laboratory (LANL), 2002.
[6] R.E. Prael, H. Lichtenstein, User Guide to LCS: The LAHET Code Systems, LA-UR-89-3014, Los Alamos National Laboratory, 1989.
[7] Takahiro Tadokoro, Yukio Kawakubo, Hirofumi Seki, Ryuichi Tayama, Kikuo Umegaki, Mamoru Baba, Tooru Kobayashi, Feasibility study on a common use accelerator system of neutron production for BNCT and radionucline production for PET, in: Advances in Neutron Capture Therapy 2006 (Proceedings of the ICNCT-12), 2006, p. 304 .
[8] S. Tanaka, M. Fukuda, K. Nishimura, et al., A code system to calculate induced radioactivity produced by ions and neutrons, JAERI-Data/Code 97-019, 1997.
[9] J.C. Yanch, X.L. Zhou, G.L. Brownell, A Monte Carlo investigation of the dosimetric properties of monoenergetic neutron beams for neutron capture therapy, Radiat. Res. 126 (1991) 1.
[10] Y.W.H. Liu, T.T. Huang, S.H. Jiang, H.M. Liu, Renovation of epithermal neutron beam for BNCT at THOR, Appl. Radiat. Isotop. 61 (2004) 1039.
[11] Yoshinori Sakurai, Tooru Kobayashi, Characteristics of the KUR heavy water neutron irradiation facility as a neutron irradiation field with variable energy spectra, Nucl. Instr. and Meth. A 453 (2000) 569.
[12] ICRP Publication 74, Conversion Coefficients for Use in Radiological Protection Against External Radiation, 1996.
[13] D. Wessol, M. Cohen, G. Harkin, M. Rossmeier, C. Wemple, F. Wheeler, in: SERA Workshop Lab Manual, INEEL/EXT-99-00766, 1999.
[14] D.W. Nigg, C.A. Wemple, D.E. Wessol, F.J. Wheeler, SERA-an advanced treatment planing system for neutron capture therapy and BNCT, Trans. Am. Nucl. Soc. 80 (1999) 66.

[15] Yoshinori Sakurai, Koji Ono, Improvement of dose distribution by central beam shielding in boron neutron capture therapy, Phys. Med. Biol. 52 (2007) 7409.
[16] R. Mayer, P. Sminia, Reirradiation tolerance of the human brain, Int. J. Radiat. Oncol. Biol. Phys. 70 (2008) 1350.
[17] J.F. Fowler, W.A. Tome, J.D. Fenwick, M.P. Mehta, A challenge to traditional radiation oncology, Int. J. Radiat. Oncol. Biol. Phys. 60 (2004) 1241.
[18] G.E. Laramore, F.J. Wheeler, D.E. Wessol, K.J. Stelzer, T.W. Griffin, A tumor control curve for malignant gliomas derived from fast neutron radiotherapy data: implications for treatment delivery and compound selection, advances in neutron capture therapy, in: Proceedings of the Seventh International Symposium on Neutron Capture Therapy for Cancer, 2007, p. 580.

J. Radiat. Res., 50, 377–382 (2009) Technical Report

A Simple and Rapid Method for Measurement of ^{10}B-*para*-Boronophenylalanine in the Blood for Boron Neutron Capture Therapy Using Fluorescence Spectrophotometry

Genro KASHINO[1], Satoshi FUKUTANI[2], Minoru SUZUKI[1], Yong LIU[1], Kenji NAGATA[1], Shin-Ichiro MASUNAGA[1], Akira MARUHASHI[1], Hiroki TANAKA[3], Yoshinori SAKURAI[3], Yuko KINASHI[4], Noriko FUJII[5] and Koji ONO[1]*

Boron/Neutron/Capture/Therapy.

Background and Purpose; ^{10}B deriving from ^{10}B-*para*-boronophenylalanine (BPA) and ^{10}B-borocaptate sodium (BSH) have been detected in blood samples of patients undergoing boron neutron capture therapy (BNCT) using prompt gamma ray spectrometer or Inductively Coupled Plasma (ICP) method, respectively. However, the concentration of each compound cannot be ascertained because boron atoms in both molecules are the target in these assays. Here, we propose a simple and rapid method to measure only BPA by detecting fluorescence based on the characteristics of phenylalanine. *Material and Methods;* ^{10}B concentrations of blood samples from human or mice were estimated by the fluorescence intensities at 275 nm of a BPA excited by light of wavelength 257 nm using a fluorescence spectrophotometer. *Results;* The relationship between fluorescence to increased BPA concentration showed a positive linear correlation. Moreover, we established an adequate condition for BPA measurement in blood samples containing BPA, and the estimated ^{10}B concentrations of blood samples derived from BPA treated mice were similar between the values obtained by our method and those by ICP method. *Conclusion;* This new assay will be useful to estimate BPA concentration in blood samples obtained from patients undergoing BNCT especially in a combination use of BSH and BPA.

INTRODUCTION

^{10}B-*para*-boronophenylalanine (BPA) and ^{10}B-borocaptate sodium (BSH) have been used for boron neutron capture therapy (BNCT).[1–5] ^{10}B nucleus has markedly large cross section to capture slow neutrons in comparison with body composition elements. The ^{10}B (n, α) ^{7}Li reaction releases a high linear energy transfer (LET) α particle and a recoiling ^{7}Li ion with an average total kinetic energy of 2.34 MeV. Their tracks do not exceed one cell diameter. Therefore if these compounds accumulate in tumour cells or tumour tissue and they receive thermal neutrons or epi-thermal neutrons, the tumours can be destroyed efficiently and selectively. As the effectiveness of BNCT is related primarily to the selective accumulation of the boron compounds in the tumor relative to the surrounding normal tissues, concentration of boron compounds should be monitored carefully for efficient killing of the tumour cells. In the clinical setting of BNCT, the ^{10}B concentration in blood should be monitored to estimate radiation dose delivered to tumour and normal tissues. As previously reported, BPA and BSH are combined to ensure such efficient killing.[6–10] The relative BNCT effect varies depending on the combination of ^{10}B compound and tissue or organ even at a same ^{10}B concentration and neutron fluence. This effective RBE has been determined by experiments on each normal tissue assuming that ^{10}B compound is distributing in the tissue at equal concentration in blood. ^{10}B concentration in blood has been measured by prompt gamma ray spectrometer, or ICP method.[11–13] However,

*Corresponding author: Phone: +81-72-451-2475,
Fax: +81-72-451-2627,
E-mail: onokoji@rri.kyoto-u.ac.jp

[1]Particle Radiation Oncology Research Centre, Research Reactor Institute, Kyoto University; [2]Laboratory of Radioactive Waste Management, Research Reactor Institute, Kyoto University; [3]Laboratory of Radiation Medical Physics, Research Reactor Institute, Kyoto University; [4]Laboratory of Radiation Safety and Control, Research Reactor Institute, Kyoto University; [5]Laboratory of Radiation Biochemistry and Biological function, Research Reactor Institute, Kyoto University.
doi:10.1269/jrr.09015

these methods can not distinguish ^{10}B concentration of BPA and BSH in blood samples. Therefore, a simple and rapid method to measure ^{10}B concentration of each compound separately is needed to accurately estimate X-ray equivalent dose. We proposed a simple and rapid method to measure only BPA by detecting fluorescence at 275 nm of a BPA compound excited by light of wavelength 257 nm using a fluorescence spectrophotometer based on the characteristics of phenylalanine.

MATERIALS AND METHODS

Measurement of BPA concentration in ethanol

A stock solution of BPA (1,300 or 1,600 ppm ^{10}B) was used for all experiments. BPA solutions were diluted with ethanol, and 1 ml solution was poured into the cuvette and placed in the cell of the fluorescence spectrophotometer (F-2000; Hitachi, Tokyo, Japan). The fluorescence spectrophotometer was set at 700 V for detection amplification. Excitation and emission wavelengths were 257 nm and 275 nm, respectively. These wavelengths were determined from the fact that phenylalanine can be measured in these wavelength with little influence by the other amino acids such as tyrosine and tryptophan.[14] This was evidenced in Fig 2a.

Measurement of BPA concentration in human blood

Blood samples obtained from a healthy man volunteer (35 years old) was analysed within 24 h. An aliquot of 200 µl of blood was added to each 1.5 ml tube, and 1–10 µl of BPA (6.5–65 ppm ^{10}B) and 1.2 µl of BSH (30 ppm ^{10}B) stock solution were added to the blood samples. After vortex-mixing the sample for a few seconds, blood was centrifuged at 15,000 rpm for 2 minutes, and 50 µl of the supernatant containing plasma fraction was poured in another 1.5 ml tube. A 12-fold volume of ethanol (600 µl) was added to the plasma and the tube was vortex-mixed. Samples were centrifuged at 15,000 rpm for 2 minutes. After centrifugation, supernatants were poured into the collection tube, which was part of a syringeless filter device (Mini-Uniprep, Whatman, NJ, USA). The solution was pushed through polytetrafluoroethylene filter media (pore size, 0.45 µm) to remove proteins present in the plasma solution. Filtrated solutions were diluted with ethanol to concentrations (10-, 20- and 25-fold), and 1 ml solutions were poured into the cuvette and placed in the cell of the fluorescence spectrophotometer.

Measurement of BPA concentration in mice blood

BPA solution (0.3 or 0.6 ml of 1,600 ppm ^{10}B) was administrated intraperitoneally to C3H mice. Twenty minutes after injection of BPA, 0.3 ml of heparin solution (1,000 unit/ml of heparin sodium solution, Ajinomoto, Tokyo, Japan) was injected. Five minutes after injection of heparin, 500–1,000 µl of blood was collected from the eye's artery. An aliquot of 50 µl of blood was added to each 1.5 ml tube, and 0.5–1.5 µl of BPA (16–48 ppm ^{10}B) were added to the blood samples. After vortex-mixing the sample for a few seconds, blood was centrifuged at 15,000 rpm for 2 minutes, and 20 µl of the supernatant containing plasma fraction was poured in another 1.5 ml tube. A 12-fold volume of ethanol (240 µl) was added to the plasma and the tube was vortex-mixed. Samples were centrifuged at 15,000 rpm for 2 minutes. After centrifugation, supernatants were poured into the collection tube, which was part of a syringeless filter device (Mini-Uniprep, Whatman, NJ, USA). The solution was pushed through polytetrafluoroethylene filter media (pore size, 0.45 µm) to remove proteins present in the plasma solution. Filtrated solutions were diluted with ethanol to concentrations (20-fold), and 1 ml solutions were poured into the cuvette and placed in the cell of the fluorescence spectrophotometer.

ICP method

Plasma samples were obtained after centrifugation of human and mice blood as described previously. Twenty micro-litter of plasma were diluted with 5 ml water and stored in the fridge. Inductively Coupled Plasma (ICP) method was performed as following the recommended instruction. The concentration of boron in each plasma sample was determined by ICPS-1000TR (Shimazu, Kyoto, Japan).

RESULTS AND DISCUSSION

The relationship between BPA concentration in ethanol and fluorescence showed a positive linear correlation until high intensities of fluorescence were achieved (Fig. 1). Our measurement condition was therefore suitable for detecting

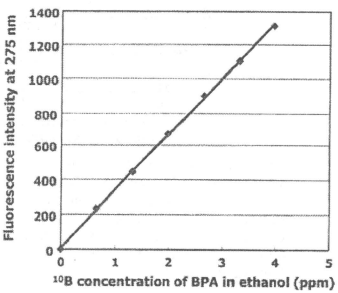

Fig. 1. Relationship between BPA concentration and fluorescence intensity at 275 nm in ethanol. The fluorescence value of only ethanol was subtracted at all points. The equation of this line was $y = 332 x + 9.26$ ($R^2 = 0.9996$).

BPA concentration without fluorescence saturation. A similar slope for the scattered plot was obtained if water or phosphate-buffered solution was used instead of ethanol as the solvent (data not shown), suggesting that soluble BPA was detected without the influence of solvents. Ethanol, even in the absence of BPA, emits fluorescence at 275 nm after excitation by light at 257 nm. The value for ethanol without BPA was 130–180 and the obtained fluorescence value of only ethanol was subtracted from the total fluorescence value of BPA and ethanol solution.

Despite the influences of many fractions in blood, only BPA should be measured in this method. The fluorescence spectrum between 260 and 360 nm excited by the light 257 nm were shown in Fig 2a. The spectrums for the samples derived from human plasma without BPA (dark blue) were clearly different from the spectrum for ethanol only. This suggests that plasma only emit the light (especially in over 280 nm). However, the light 275 nm were not influenced by the fractions of plasma and increased intensities in 275 nm were observed with higher concentration of BPA (Fig 2a). The scattered plots of the samples derived from human blood before subtraction of the ethanol intensities and after subtraction of those were shown on the left (b) and right (c) of Fig. 2, respectively. In the sample without BPA addition (0 ppm), fluorescence was the same as the intensity of ethanol when used alone (zero in Fig. 2c), suggesting that

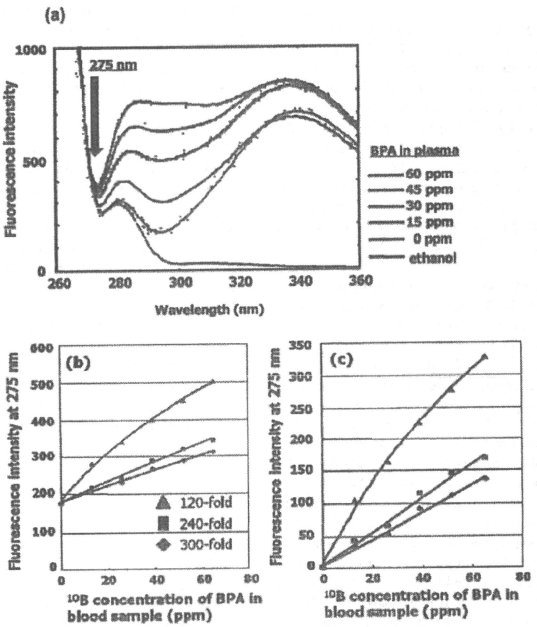

Fig. 2. (a) The fluorescence spectrum between 260 and 360 nm excited by the light 257 nm in BPA added plasma samples. (b)(c) Relationship between BPA concentration and fluorescence intensity at 275 nm in blood samples. (b) Scattered plots before subtraction of the fluorescence value for only ethanol, and (c) after subtraction of the fluorescence value for only ethanol. The data from the three ratios for dilution of blood samples are represented as follows: 120-fold: yellow triangle; 240-fold: pink square and 300-fold: blue diamond. The equations of lines for the scattered plots from 120-, 240- and 300-fold dilution were $y = -0.0303\ x^2 + 6.82\ x + 183.24$ ($R^2 = 0.9968$), $y = 2.5963\ x + 178.87$ ($R^2 = 0.9908$) and $y = 2.0538\ x + 178.33$ ($R^2 = 0.9929$), respectively.

all other components which influence measurement at 275 nm were excluded by our treatments. When the samples were prepared for measurement, plasma samples were diluted with ethanol. We diluted the samples at three types of ratio. Slope values decreased according to the dilution ratio. In case of 120-fold dilution, the shape of the line was quadratic at < 65 ppm ^{10}B of BPA. The reason for as to why the scattered plots reached the ceiling at lower dilution ratio is unclear, but linear increase with 2.1 and 2.6 of slope value was observed in 300-fold and 240-fold dilution samples, respectively. This slope value means that the range of resolution is < 0.5 ppm ^{10}B in BPA containing blood sample. We therefore applied a 240-fold dilution in the further study.

To mimic the blood sample of a patient undergoing BNCT, BPA containing blood sample at 13 ppm ^{10}B was previously prepared for creating scattered plots, in addition to the control scattered plots between ^{10}B of BPA concentra-

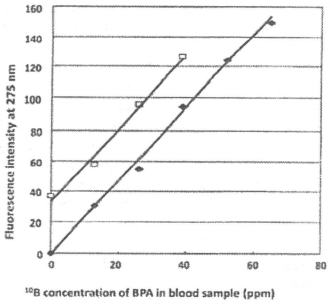

Fig. 3. Relationship between BPA concentration and fluorescence intensity at 275 nm in blood samples with (white square) and without (black diamond) previous addition of 13 ppm BPA. The dilution ratio of all blood samples was 240-fold. The equations of lines for the scattered plots from blood samples with previous addition of BPA (white square) and control (black diamond) were $y = 2.3654 x + 32.85$ ($R^2 = 0.988$) and $y = 2.3479 + 0.7905$ ($R^2 = 0.9966$), respectively.

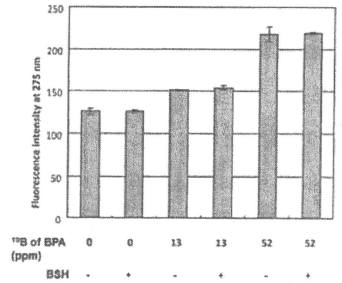

Fig. 4. Little effects were observed by the presence of BSH on BPA measurement in the blood samples. Thirty ppm ^{10}B of BSH was added to blood sample containing BPA in each concentration. Result shows mean frequency ± standard error of the mean (SEM) of fluorescence intensities from three independent experiments.

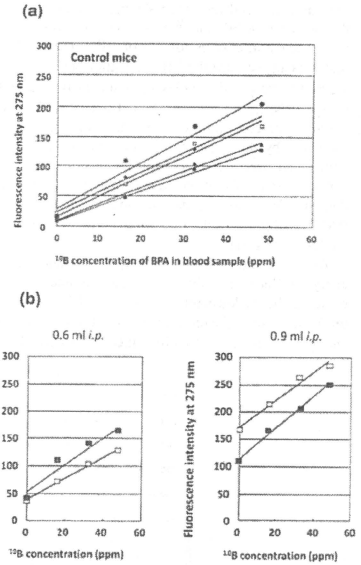

Fig. 5. (a) Relationship between BPA concentration and fluorescence intensity at 275 nm in blood samples derived from five non-treated mice. The equations of lines for the scattered plots from each mouse sample were $y = 3.9775 x + 27.49$ ($R^2 = 0.9607$), $y = 3.3981 x + 14.92$ ($R^2 = 0.9877$), $y = 3.3906 x + 22.55$ ($R^2 = 0.9965$), $y = 2.72 x + 9.97$ ($R^2 = 0.9945$), $y = 2.5338 x + 7.84$ ($R^2 = 0.9959$), respectively. (b) Relationship between added BPA concentration and fluorescence intensity at 275 nm in blood samples derived from mice treated with 0.6 ml (left) and 0.9 ml (right) BPA solutions. The equations of lines for the scattered plots from the samples of 0.6 ml and 0.9 ml treated mouse were $y = 2.4069 x + 54.11$ ($R^2 = 0.9442$) (black plots of left panel), $y = 1.8869 x + 39.69$ ($R^2 = 0.9923$) (white plots of left panel), and $y = 2.5719 x + 170.45$ ($R^2 = 0.9782$) (white plots of right panel), $y = 2.93 x + 112.33$ ($R^2 = 0.9982$) (black plots of right panel), respectively.

tions and fluorescence intensities. Two nearly parallel linear scattered plots were obtained between the control and the BPA-added sample (Fig. 3). The equations of lines for the scattered plots from blood samples with previous addition of BPA (white square) and control (black diamond) were $y = 2.3654\ x + 32.85$ ($R^2 = 0.988$) and $y = 2.3479\ x + 0.7905$ ($R^2 = 0.9966$), respectively. Therefore, the slope value was indicated to be almost equal (2.3654 vs 2.3479). It was indicated that the increased fluorescence intensity in the sample with previous addition of BPA was 32.06 at the y intercept after subtraction of background y value. The estimated BPA concentration in the sample was 13.55 ppm (32.06 was divided by 2.3654, slope for pink plots). This estimated value is very similar with 13 ppm as an actual concentration.

Also, we examined the influence of BSH on our BPA measurement, and the result showed that no influences by the presence of 30 ppm ^{10}B of BSH were observed in the fluorescence intensities for ^{10}B of BPA (Fig. 4). It is clear that we can measure the ^{10}B concentrations of BPA by this method using blood samples simultaneously containing two compounds. In the present clinical use of BPA with BSH, approximate concentrations for each compound have been estimated by the expected concentrations for ^{10}B of BSH, which had been obtained from attenuation curve of BSH concentrations. Therefore, the results are clearly showing that an application of our method to clinical setting for BNCT will improve the measurement of ^{10}B concentrations for BPA and BSH.

To mimic the patient situation, BPA treated mice were analysed. Because of the small blood volume, we could not estimate the background intensity in a BPA treated mouse unlike in human. Therefore, we first estimated an average of background intensity from five mice. BPA was added in the blood samples derived from five mice, and five linear lines followed by scattered plots were drawn with a good correlation (Fig. 5a). The reason why the slopes of each line in control mice were discord should be because of different hematocrit values among mice, as BPA must be distributed to plasma fraction. The average of the y intercepts from five values (between 7.84 and 27.49) was 16.55 (Fig. 5a). The y intercepts in mice samples were higher than those in human blood, because fluorescence may be emitted from heparin. In the preparation of mice samples, heparin is needed to collect the blood without blood-curdling into a tube. In contrast, human blood was collected into tube containing EDTA-2Na and this is not influent in the fluorescent intensities of samples (data not shown). Next, scattered plots were described in BPA treated mouse (Fig. 5b). The left and right graphs are showing that the 0.6 and 0.9 ml of BPA stock (1,600 ppm ^{10}B of BPA) were administrated intraperitoneally, respectively. The y intercepts in the lines of the left graph (Fig. 5b, black and white plots) were 54.11 and 39.69. The values after the subtraction of background value (16.55) were 23.14 and 37.56, respectively; therefore, the BPA concentrations from the lines were 12.26 ppm and 15.61 ppm (divided by each slope value 1.8869 and 2.4069, respectively). In the right graph of Fig. 5b, the values at the y intercept in black and white plots were 95.78 and 153.9 after the subtraction of background value, respectively. Therefore, concentrations in 0.9 ml treated mice were 32.69 ppm and 59.84 ppm, respectively.

We next compared our new method to ICP method in the measurement of blood concentration of ^{10}B in BPA treated mice. As shown in the left graph of Fig. 6, good correlation was observed between fluorescence intensities and ^{10}B concentrations for BPA. In the graph, the y intercept was 56.637, and the value after the subtraction of background

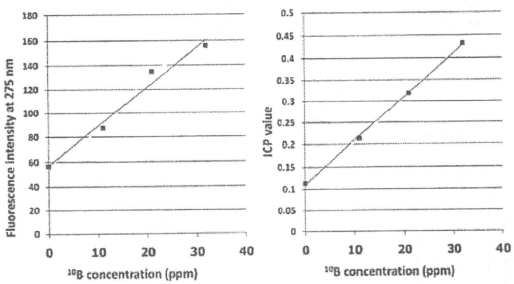

Fig. 6. The comparison of the new method and ICP method in the samples derived from a BPA treated mouse. Left panel is showing the relationship between fluorescence intensity and added BPA concentration. The equations of lines for the scattered plots were $y = 3.2477\ x + 56.637$ ($R^2 = 0.9756$). Right panel is showing the relationship between the relative values for boron evaluated by ICP and added BPA concentration from the same mouse. The equation of line for the scattered plots was $y = 0.01\ x + 0.109$ ($R^2 = 0.9988$).

intensity, 16.55 (obtained from Fig. 5a) was 40.087. Therefore, the estimated concentration after divided by 3.2477 (slope value) was 12.34 ppm. As well as the left graph, good correlations were observed between ICP value and ^{10}B concentrations for BPA. In the graph, the y intercept was 0.109. The background value in ICP was almost zero; therefore, estimated concentration after divided by 0.01 (slope value) was 10.9 ppm. It is clearly shown that the difference between the two estimated concentrations in each method is small (12.34 ppm vs 10.9 ppm). There is still difference of 1.44 ppm, but this difference may be mainly brought by the dispersion of background values in mice experiment as shown in Fig. 5a. In the estimation of background fluorescence intensity in mice, we set the average background value, 16.55, from five mice data of Fig. 5a. However, this is not actual background value for each BPA treated mouse. If we could collect the blood to estimate the background level before BPA treatment in the same mouse, more exact BPA concentration should be detected. In the case of a patient, it is possible to collect the blood just before the BPA treatment for a detection of the background level of each patient. Therefore, exact ^{10}B concentrations of BPA can be estimated by our new method in BPA treated patient as well as ICP method.

CONCLUSION

We established a new method to measure only BPA in blood sample by detecting fluorescence based on the characteristics of phenylalanine. This method will be especially useful for BPA measurement in patients undergoing BNCT by concomitant use of BPA and BSH.

ACKNOWLEDGEMENT

The authors are grateful to Yuka Yamamoto for taking blood samples. This research was supported by the grant of Initiative for Nuclear Fundamental Strategic Research.

REFERENCES

1. Mishima, Y., Honda, C., Ichihashi, M., Obara, H., Hiratsuka, J., Fukuda, H., Karashima, H., Kobayashi, T., Kanda, K. and Yoshino, K. (1989) Treatment of malignant melanoma by single thermal neutron capture therapy with melanoma-seeking 10B-compound. *Lancet* **2**: 388–389.
2. Hatanaka, H. (1991) Boron-Neutron Capture Therapy for tumors, in "Glioma", A. Karim & ER. Laws. Ed. Springer-Verlag, Berlin, New York. 233–270.
3. Kato, I., Ono, K., Sakurai, Y., Ohmae, M., Maruhashi, A., Imahori, Y., Kirihata, M., Nakazawa, M. and Yura, Y. (2004) Effectiveness of BNCT for recurrent head and neck malignancies. *Appl. Radiat. Isot.* **61**: 1069–1073.
4. Aihara, T., Hiratsuka, J., Morita, N., Uno, M., Sakurai, Y., Maruhashi, A., Ono, K. and Harada, T. (2006) First clinical case of boron neutron capture therapy for head and neck malignancies using ^{18}F-BPA PET. *Head Neck.* **28**: 850–852.
5. Suzuki, M., Sakurai, Y., Hagiwara, S., Masunaga, S., Kinashi, Y., Nagata, K., Maruhashi, A., Kudo, M. and Ono, K. (2007) First attempt of boron neutron capture therapy (BNCT) for hepatocellular carcinoma, *Jpn. J. Clin. Oncol.* **37**: 376–381.
6. Ono, K., Masunaga, S., Kinashi, Y., Takagaki, M., Akaboshi, M., Kobayashi, T. and Akuta, K. (1996) Radiobiological evidence suggesting heterogeneous microdistribution of boron compounds in tumors: its relation to quiescent cell population and tumor cure in neutron capture therapy. *Int. J. Radiat. Oncol. Biol. Phys.* **34**: 1081–1086.
7. Ono, K., Masunaga, S., Suzuki, M., Kinashi, Y., Takagaki, M. and Akaboshi, M. (1999) The combined effect of boronophenylalanine and borocaptate in boron neutron capture therapy for SCCVII tumors in mice. *Int. J. Radiat. Oncol. Biol. Phys.* **43**: 431–436.
8. Barth, R. F., Yang, W., Rotaru, J. H., Moeschberger, M. L., Boesel, C. P., Soloway, A. H., Joel, D. D., Nawrocky, M. M., Ono, K. and Goodman, J. H. (2000) Boron neutron capture therapy of brain tumors: enhanced survival and cure following blood-brain barrier disruption and intracarotid injection of sodium borocaptate and boronophenylalanine. *Int. J. Radiat. Oncol. Biol. Phys.* **47**: 209–218.
9. Kawabata, S., Miyatake, S., Kuroiwa, T., Yokoyama, K., Doi, A., Iida, K., Miyata, S., Nonoguchi, N., Michiue, H., Takahashi, M., Inomata, T., Imahori, Y., Kirihata, M., Sakurai, Y., Maruhashi, A., Kumada, H. and Ono, K. (2009) Boron neutron capture therapy for newly diagnosed glioblastoma. *J. Radiat. Res.* **50**: 51–60.
10. Miyatake, S., Kawabata, S., Kajimoto, Y., Aoki, A., Yokoyama, K., Yamada, M., Kuroiwa, T., Tsuji, M., Imahori, Y., Kirihata, M., Sakurai, Y., Masunaga, S., Nagata, K., Maruhashi, A. and Ono, K. (2005) Modified boron neutron capture therapy for malignant gliomas performed using epithermal neutron and two boron compounds with different accumulation mechanisms: an efficacy study based on findings on neuroimages. *J. Neurosurg.* **103**: 1000–1009.
11. Takagaki, M., Oda, Y., Miyatake, S., Kikuchi, H., Kobayashi, T., Sakurai, Y., Osawa, M., Mori, K. and Ono, K. (1997) Boron neutron capture therapy: preliminary study of BNCT with sodium borocaptate (Na2B1 2H1 1SH) on glioblastoma. *J Neurooncol.* **35**: 177–185.
12. Munck af Rosenschöld, P. M., Verbakel, W. F., Ceberg, C. P., Stecher-Rasmussen, F. and Persson, B. R. (2001) Toward clinical application of prompt gamma spectroscopy for in vivo monitoring of boron uptake in boron neutron capture therapy. *Med Phys.* **28**: 787–795.
13. Hiratsuka, J., Yoshino, K., Kondoh, H., Imajo, Y. and Mishima, Y. (2000) Biodistribution of boron concentration on melanoma-bearing hamsters after administration of *p*-, *m*-, *o*-boronophenylalanine. *Jpn. J. Cancer Res.* **91**: 446–450.
14. Biochemical Data Book, pp43, Tokyo Kagaku Dojin.

Received on February 9, 2009
Revision received on April 2, 2009
Accepted on April 9, 2009
J-STAGE Advance Publication Date: June 9, 2009

J. Radiat. Res., 50, 553–557 (2009)

Regular Paper

γ-ray Irradiation Enhanced Boron-10 Compound Accumulation in Murine Tumors

Yong LIU[1†], Kenji NAGATA[1,2†], Shin-ichiro MASUNAGA[1], Minoru SUZUKI[1], Genro KASHINO[1], Yuko KINASHI[1], Hiroki TANAKA[1], Yoshinori SAKURAI[1], Akira MARUHASHI[1] and Koji ONO[1*†]

Irradiation/γ-ray/BSH/SCCVII/Mice.

Previous studies have demonstrated that X-ray irradiation affects angiogenesis in tumors. Here, we studied the effects of γ-ray irradiation on boron-10 compound accumulation in a murine tumor model. The mouse squamous cell carcinoma was irradiated with γ-ray before BSH (^{10}B-enriched borocaptate sodium) administration. Then, the boron-10 concentrations in tumor and normal muscle tissues were measured by prompt γ-ray spectrometry (PGA). A tumor blood flow assay was performed, and cell killing effects of neutron irradiation with various combinations of BSH and γ-rays were also examined. BSH concentrations of tumor tissues were 16.1 ± 0.6 μg/g, 16.7 ± 0.5 μg/g and 17.8 ± 0.5 μg/g at 72 hours after γ-ray irradiation at doses of 5, 10, and 20 Gy, compared with 13.1 ± 0.5 μg/g in unirradiated tumor tissues. The enhancing inhibition of colony formation by neutron irradiation with BSH was also found after γ-ray irradiation. In addition, increasing Hoechst 33342 perfusion was also observed. In this study, we demonstrated that γ-ray irradiation enhances BSH accumulation in tumors. The present results suggest that the enhancement of ^{10}B concentration that occurs after γ-ray irradiation may be due to the changes in the extracellular microenvironment, including in tumor vessels, induced by γ-ray irradiation.

INTRODUCTION

The potential advantage of boron neutron capture therapy (BNCT) has been demonstrated in the treatment of cancer because of its selective destroying tumor cells.[1–4] In essence, a non-cytotoxic boron-10 compound that is considered to be selectively enriched in tumor cells is administered. During the subsequent irradiation of thermal neutrons, ^{10}B captures neutrons and emits high-energy α and ^{7}Li particles. The emitted particles have high energy (2.79 MeV) and short paths (≤ 10 μm). Since the path length is nearly the same as the length of a cell, it can selectively destroy tumor cells without affecting the surrounding normal tissues.

The efficiency of BNCT is mostly based on the ^{10}B distribution in tumor cells. Many studies have focused on the delivery of ^{10}B to tumors,[5] including via the boron delivery system.[6] However, tumors vessels are more permeable than the vessels of normal tissues.[7] The abnormal structure of tumor vessels leads to a decreased uptake of drugs into tumors.[8] Thus the improvement of tumor blood flow is important for delivering ^{10}B to tumors.

It has been demonstrated that irradiation can induce cellular, biochemical, and molecular changes in tumor cells, resulting in cell death.[9,10] In addition, the effect of irradiation on the tumor microenvironment has also been reported.[11] Previous studies have suggested that ionizing radiation can modulate tumor vasculature functionality and promote the selective delivery of drugs to tumors.[12] However, the effect of irradiation on tumor vessels is not completely understood. Here, we investigated the effect of irradiation of γ-ray on ^{10}B concentration in a mouse squamous cell carcinoma model.

MATERIALS AND METHODS

Cell culture and tumor model

Cells of the mouse squamous cell carcinoma cell line SCCVII (Department of Radiology, Kyoto University) were cultured in Eagle's minimum essential medium supplemented with 15% fetal calf serum and 292 mg/l glutamine at 37°C in an atmosphere of 95% air and 5% CO_2.

*Corresponding author: Phone: +81-724-51-2475.
Fax: +81-724-51-2627.
E-mail: onokoji@rri.kyoto-u.ac.jp
[1]Research Reactor Institute, Kyoto University, 2-1010 Asashiro-nishi, Kumatori-cho, Sennan-gun, Osaka 590-0494; [2]Department of Radiology, Ishikiriseiki Hospital, 18-28 Yayoi-cho, Higashiosaka 579-8062, Japan.
†Yong LIU, Kenji NAGATA and Koji ONO contributed equally to this work.
doi:10.1269/jrr.09071

SCCVII cells were collected from exponentially growing cultures, and approximately 2.0×10^5 cells were inoculated subcutaneously into the hind legs of 8- to 9-week-old C3H/He female mice. Fourteen days after tumor inoculation, the tumors had reached approximately 10 mm in diameter. All animal experiments were carried out in accordance with the Guidelines for Animal Experimentation of the Research Reactor Institute of Kyoto University.

Gamma-ray irradiation

Gamma-ray irradiation was produced using a cobalt-60 γ-ray irradiator at a dose rate of 0.5 Gy/min. The unanesthetized mice were confined to plastic jigs, and irradiation was applied locally to the hind leg in which the tumor had been transplanted. The rest of body was shielded by lead. The irradiation was performed with a single dose of 5, 10, or 20 Gy.

Thermal neutron irradiation

The tumors were excised 30 min after BSH administration. The tumor tissues were placed into Teflon tubes, and then thermal neutron irradiation containing a negligible amount of fast neutrons was started within 10 min of the tumor excision at the heavy water facility of Kyoto University Reactor (KUR). The cadmium ratio of the thermal neutron beam was 148 including 2×10^9 n/cm·sec thermal, 1.4×10^7 n/cm·sec epithermal and 2.8×10^6 n/cm·sec fast neutron fluxes. The fluence of the neutrons that reached the tissue was measured by γ-ray spectrometry, and the results are shown as the mean arithmetic value.

Boron-10 compound and measurement of the boron-10 concentration

The boron-10 compound BSH was purchased from Katchem., Ltd. (Czech Republic) and was dissolved in physiological saline. BSH was administered (75 mg/kg, i.p.) from 3 hours to 96 hours after γ-ray irradiation. The tumors and surrounding normal muscle tissues were obtained 30 min after the administration of BSH. The ^{10}B concentrations were measured by prompt γ-ray (PGA) spectrometry using a thermal neutron guide tube installed at KUR.

Colony formation assay

The clonogenic cell survival assay was performed using *in vivo-in vitro* assay.[13] The tumors exposed to neutron irradiation were minced with scissors, and single cell suspensions were obtained by digesting tumor fragments with a mixed solution of 0.05% trypsin and 0.02% EDTA at 37°C for 15 min. Appropriate concentrations of live tumor cells were seeded in 60 mm dishes containing complete fresh medium. After incubation for 10 days, the colonies were fixed with 70% ethanol, stained with crystal violet, and counted. Tumor tissues kept in Teflon tubes without neutron exposure were used as controls. To determine the surviving cell fraction (SF), the plating efficiency following neutron irradiation was divided by that of control tumors.

Analysis of blood perfusion

To determine the effect of γ-ray irradiation on blood perfusion in tumors, the perfusion marker Hoechst 33342 (Sigma-Aldrich, MO) was used. Hoechst 33342 (16 mg/kg) was injected via the tail vein 1 min before tumor excision. Then the tumor tissue was obtained and flash-frozen in O.C.T mounting medium with liquid nitrogen. Sections were cut into 10 μm-thick slices and mounted on slide glasses using 50% glycerol containing propidium iodide (PI) (1:500). All images were obtained using a fluorescence microscope (BZ-9000, KEYENCE, Japan).

Statistical analysis

Data are presented as the mean ± standard error (SE). Statistical analyses were performed using the Student's *t*-test to compare with the differences between the groups with StatView J-5.0 software. P values < 0.05 were considered statistically significant.

RESULTS

Quantitative analysis of ^{10}B concentration in tumors after γ-ray irradiation

The ^{10}B concentrations of tumors after γ-ray irradiation were analyzed by PGA (Fig. 1). As shown in Fig. 1, the tumor ^{10}B concentrations were 16.1 ± 0.6 μg/g, 16.7 ± 0.5 μg/g and 17.8 ± 0.5 μg/g at 72 hours after γ-ray irradiation

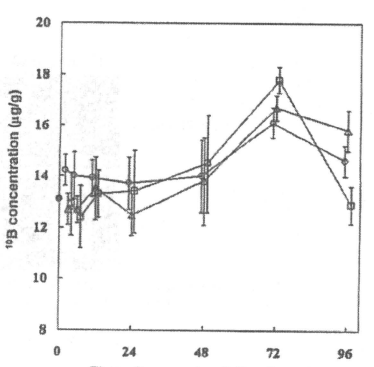

Fig. 1. Change in ^{10}B concentration in tumors after γ-ray irradiation. (●) BSH alone, (○) γ-ray 5 Gy + BSH, (△) γ-ray 10 Gy + BSH, (□) γ-ray 20 Gy + BSH. The points represent the mean value (± SE) for five to eleven tumors.

with doses of 5, 10 and 20 Gy, respectively. These concentrations were increased significantly ($p < 0.01$) compared with the value of the unirradiated control tumor (13.1 ± 0.5 μg/g).

Effect of γ-ray irradiation on the surviving fractions of SCCVII cells

Cell survival curves after neutron irradiation are shown in Fig. 2. The surviving fractions decreased with increasing of neutron fluence. The curves of the surviving fractions (SF) were as follows: neutron irradiation alone ($SF = e^{-0.5725x}$), neutron irradiation with γ-ray irradiation ($SF = e^{-0.3800x}$), BNCT (75 mg) without γ-ray irradiation ($SF = e^{-0.8117x}$), and BNCT (75 mg) with γ-ray irradiation ($SF = e^{-0.9499x}$). The SF with BSH was decreased compared to those without BSH. In addition, the fractions of BNCT that received γ-ray irradiation of 5 Gy were significantly decreased compared with those exposed to BNCT alone without γ-ray irradiation. These results showed that (1) the combination of neutrons and boron was effective at inhibiting tumor cell growth, and (2) γ-ray irradiation can contribute to the accumulation of ^{10}B in tumor cells.

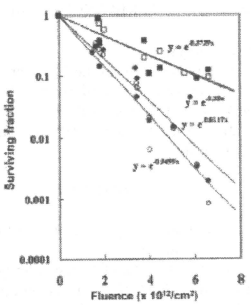

Fig. 2. Surviving fractions of SCCVII cells after neutron irradiation. (■) no γ-ray + no BSH, (□) γ-ray 5 Gy alone (●) BSH alone, (○) γ-ray 5 Gy + BSH. The points represent the mean value for five to eleven tumors.

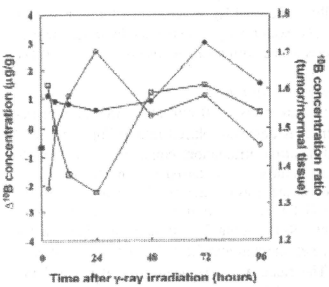

Fig. 3. Change in ^{10}B concentration after γ-ray irradiation in tumors and normal tissues. (●) γ-ray 5 Gy + BSH, in tumor tissue, (○) γ-ray 5 Gy + BSH, in normal tissue, (□) γ-ray 5 Gy + BSH, tumor tissues/normal tissues, (■) BSH alone, tumor tissues/normal tissues. The points represent the mean value for five to eleven tumors.

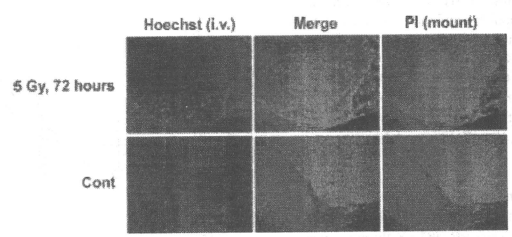

Fig. 4. Representative images of Hoechst 33342 distribution in tumors after γ-ray irradiation. Hoechst 33342 is shown as blue, PI is shown as red and the merged image is shown as pink. Cont: without γ-ray irradiation. Magnification: × 40.

Effect of γ-ray irradiation on the boron-10 concentration in tumors and normal muscle tissues

The ^{10}B concentrations of tumors and normal muscle tissues that did not receive γ-ray irradiation were 13.1 ± 0.5 μg/g (n = 52) and 9.7 ± 1.4 μg/g (n = 52), respectively. After 5 Gy of γ-ray irradiation, the ^{10}B concentration of the tumors was increased with the increase reaching a peak of 3.0 μg/g at 72 hours after irradiation. In the normal muscle tissue, the ^{10}B concentration of normal muscle tissues was increased quickly with the increase reaching a peak of 2.7 μg/g at 24 hours after irradiation, and then decreased to the unirradiated level by 96 hours after irradiation. The ratio of ^{10}B concentration in the tumor to that in normal muscle tissues was also increased to 1.61 at 72 hours after irradiation compared to the value of 1.45 observed at 24 hours after irradiation (Fig. 3).

Effect of γ-ray irradiation on tumor blood perfusion

Tumor blood perfusion was investigated by observing the distribution of the perfusion marker Hoechst 33342. The size of the Hoechst 33342 positive regions had increased markedly 72 hours after γ-ray irradiation with 5 Gy compared with those in the unirradiated control (Fig. 4), suggesting that γ-ray irradiation improves the blood perfusion in tumors.

DISCUSSION

BNCT is a tumor cell targeted radiation therapy, the benefit of which is based on the highly selective distribution of ^{10}B in tumor cells.[14] The delivery of ^{10}B to tumors is considered as the key to the success of BNCT.[15,16]

However, tumor vessels have different structures and functions from normal vasculature. These abnormalities are found in blood vessel size, shape, perfusion, and the components of the vessel wall. In addition, a lack of vascular density is also found in the central areas of tumors, resulting in the insufficient delivery of oxygen and drugs into tumors.[8,17] Therefore, improving the blood supply to tumors including via normalization of tumor vasculature might be applied to BNCT. A pervious study in a murine tumor model showed that tumor irradiation was abe to induce angiogenesis through the up-regulation of the nitric oxide pathway.[18] In this study, we investigated the effect of γ-ray irradiation before BNCT on ^{10}B concentration in tumors. It was demonstrated that γ-ray irradiation significantly increased the ^{10}B concentration in tumor tissues at 72 hours after γ-ray irradiation (Fig. 1) and enhanced cell killing effect of BNCT (Fig. 2). In addition, an increasing ratio of ^{10}B concentration in tumors to that in normal muscle tissues was also found (Fig. 3). These indicated that pre-irradiation of γ-ray enhanced BNCT effects on tumors.

The effect of γ-ray irradiation on improving ^{10}B accumulation in tumors was demonstrated, but no γ-ray dose dependency on ^{10}B concentration was found (Fig. 1). After γ-ray irradiation of 5 Gy, ^{10}B concentration in tumor was increased immediately and stable for 48 hours. Then it was increased again and reached peak 72 hours after irradiation of γ-ray (Fig. 3). These suggested the effect of γ-ray irradiation on ^{10}B accumulation in tumors is a complex process. Tumor volume is considered as a factor that affects boron compound accumulation in tumors. However, no significant change was found in tumor volume at 72 hours after the delivery of 5 Gy of γ-ray compared with an unirradiated control tumor in our study (data is not presented here). From these results, we speculated that the improvement of ^{10}B concentration in tumors induced by irradiation may be due to the changes in tumors microenvironment rather than the changes in the tumor cells themselves.

Further studies showed the improvement of Hoechst perfusion in tumors after γ-ray irradiation (Fig. 4). These suggested the improving ^{10}B concentration in tumors may result from vasculature changes induced by γ-ray irradiation. However, this is not consistent with the common understanding of the effects of irradiation on tumor vasculature, which showed that irradiation can induce injury via endothelial apoptosis and anti-angiogenic responses.[19,20] Recent studies showed that the vascular pattern of angiogenesis was changed from a sprouting model to an intussusceptive model after irradiation treatment and anti-angiogenic therapy.[21] The switch from sprouting to intussusceptive angiogenesis[22] occurs in the transition period after irradiation, and may repair a damaged tumor vasculature and restore the blood supply to the tumor. Although the hallmarks of intussusceptive angiogenesis have been demonstrated by electron microcopy, details including the effect of tumor type, delivered dose, and time on intussusceptive angiogenesis are still unclear. These have to be clarified in order to fully understand the effect of irradiation on angiogenesis.

CONCLUSIONS

Our study demonstrated that γ-ray irradiation before BNCT is effective at improving the ^{10}B concentration in tumors. This finding is expected to increase the effectiveness of current clinical BNCT. In future, we have to investigate the changes in tumor vasculature structure and function induced by γ-ray irradiation and other methods for improving ^{10}B concentration selectively through the modification of tumor vasculature structure and function.

ACKNOWLEDGEMENTS

The authors are grateful to Mrs. Shoko Ono and Mrs. Masami Fukui for their technical assistance during the study. This research was supported by a Grant-in-Aid for Cancer Research (17016037) from the Japanese Ministry of Education, Culture, Sports, Science, and Technology (MEXT) to

K. O. and also by a Grant-in-Aid for Initiative for Nuclear Fundamental Strategic Research from the Japan Science and Technology Agency to K. O.

REFERENCES

1. Kawabata, S., Miyatake, S., Kuroiwa, T., Yokoyama, K., Doi, A., Iida, K., Miyata, S., Nonoguchi, N., Michiue, H., Takahashi, M., Inomata, T., Imahori, Y., Kirihata, M., Sakurai, Y., Maruhashi, A., Kumada, H. and Ono, K. (2009) Boron neutron capture therapy for newly diagnosed glioblastoma. J. Radiat. Res. **50**: 51–60.
2. Morita, N., Hiratsuka, J., Kondoh, H., Uno, M., Asano, T., Niki, Y., Sakurai, Y., Ono, K., Harada, T. and Imajo, Y. (2006) Improvement of the tumor-suppressive effect of boron neutron capture therapy for amelanotic amelanotic melanoma by intratumoral injection of the tyrosinase gene. Cancer Res. **66**: 3747–3753.
3. Fuwa, N., Suzuki, M., Sakurai, Y., Nagata, K., Kinashi, Y., Masunaga, S., Maruhashi, A., Imahori, Y., Kodaira, T., Tachibana, H., Nakamura, T. and Ono, K. (2008) Treatment results of boron neutron capture therapy using intra-arterial administration of boron compounds for recurrent head and neck cancer. Br. J. Radiol. **81**: 749–752.
4. Pisarev, M. A., Dagrosa, M. A. and Juvenal, G. J. (2007) Boron neutron capture therapy in cancer: past, present and future. Arq. Bras. Endocrinol. Metabol. **51**: 852–856.
5. Mehta, S. C. and Lu, D. R. (1996) Targeted drug delivery for boron neutron capture therapy. Pharm. Res. **13**: 344–351.
6. Nakamura, H. (2008) Liposomal boron delivery system for neutron capture therapy. Yakugaku Zasshi **128**: 193–208.
7. Ribatti, D., Nico, B., Crivellato, E. and Vacca, A. (2007) The structure of the vascular network of tumors. Cancer Lett. **248**: 18–23.
8. Jain, R. K. (1994) Barriers to drug delivery in solid tumors. Sci. Am. **271**: 58–65.
9. Streekumar, A., Nyati, M. K., Varambally, S., Barrette, T. R., Ghosh, D., Lawrence, T. S. and Chinnaiyan, A. M. (2001) Profiling of cancer cells using protein microarrays: Discovery of novel radiation-regulated proteins. Cancer Res. **61**: 7585–7593.
10. Prise, K. M., Pinto, M., Newman, H. C. and Michael, B. D. (2001) A review of studies of ionizing radiation-induced double-strand break clustering. Radiat. Res. **156**: 572–576.
11. Demaria, S. and Formenti, S. C. (2007) Sensors of ionizing radiation effects on the immunological microenvironment of cancer. Int. J. Radiat. Biol. **83**: 819–825.
12. Sonveaux, P., Dessy, C., Brouet, A., Jordan, B. F., Grégoire, V., Gallez, B., Balligand, J. L. and Feron, O. (2002) Modulation of the tumor vasculature functionality by ionizing radiation accounts for tumor radiosensitization and promotes gene delivery. FASEB J. **16**: 1979–1981.
13. Masunaga, S., Sakurai, Y., Suzuki, M., Nagata, K., Maruhashi, A., Kinash, Y. and Ono, K. (2004) Combination of the vascular targeting agent ZD6126 with boron neutron capture therapy. Int. J. Radiat. Oncol. Biol. Phys. **60**: 920–927.
14. Coderre, J. A., Turcotte, J. C., Riley, K. J., Binns, P. J., Harling, O. K. and Kiger W. S. 3rd. (2003) Boron neutron capture therapy: cellular targeting of high linear energy transfer radiation. Technol. Cancer Res. Treat. **2**: 355–375.
15. Wu, G., Barth, R. F., Yang, W., Lee, R. J., Tjarks, W., Backer, M. V. and Backer, J. M. (2006) Boron containing macromolecules and nanovehicles as delivery agents for neutron capture therapy. Anticancer Agents Med. Chem. **6**: 167–184.
16. Sjöberg, S., Carlsson, J., Ghaneolhosseini, H., Gedda, L., Hartman, T., Malmquist, J., Naeslund, C., Olsson, P. and Tjarks, W. (1997) Chemistry and biology of some low molecular weight boron compounds for boron neutron capture therapy. J. Neurooncol. **33**: 41–52.
17. McDonald, D. M. and Baluk, P. (2002) Significance of blood vessel leakiness in cancer. Cancer Res. **62**: 5381–5385.
18. Sonveaux, P., Brouet, A., Havaux, X., Grégoire, V., Dessy, C., Balligand, J. L. and Feron, O. (2003) Irradiation-induced angiogenesis through the up-regulation of the nitric oxide pathway: implications for tumor radiotherapy. Cancer Res. **63**: 1012–1019.
19. Fajardo, L. F. (1989) The unique physiology of endothelial cells and its implications in radiotherapy. Front. Radiat. Ther. Oncol. **26**: 96–106.
20. Garcia-Barros, M., Paris, F., Cordon-Cardo, C., Lyden, D., Rafii, S., Haimovitz-Friedman, A., Fuks, Z. and Kolesnick, R. (2003) Tumor response to radiotherapy regulated by endothelial cell apoptosis. Science **300**: 1155–1159.
21. Hlushchuk, R., Riesterer, O., Baum, O., Wood, J., Gruber, G., Pruschy, M. and Djonov, V. (2008) Tumor recovery by angiogenic switch from sprouting to intussusceptive angiogenesis after treatment with PTK787/ZK222584 or ionizing radiation. Am. J. Pathol. **173**: 1173–1185.
22. Patan, S., Munn, L. L. and Jain, RK. (1996) Intussusceptive microvascular growth in a human colon adenocarcinoma xenograft: a novel mechanism of tumor angiogenesis. Microvasc. Res. **51**: 260–272.

Received on June 19, 2009
Accepted on August 11, 2009
J-STAGE Advance Publication Date: October 3, 2009

Radiation Oncology

BioMed Central

Research

Open Access

Role of p53 mutation in the effect of boron neutron capture therapy on oral squamous cell carcinoma

Yusei Fujita[1], Itsuro Kato[1], Soichi Iwai[1], Koji Ono[2], Minoru Suzuki[2], Yoshinori Sakurai[2], Ken Ohnishi[3], Takeo Ohnishi[3] and Yoshiaki Yura*[1]

Address: [1]Department of Oral and Maxillofacial Surgery, Osaka University Graduate School of Dentistry, Osaka, Japan, [2]Particle Radiation Oncology Research Center Laboratory, Research Reactor Institute, Kyoto University, Osaka, Japan and [3]Department of Biology, School of Medicine, Nara Medical University, Nara, Japan

Email: Yusei Fujita - fujisan@dent.osaka-u.ac.jp; Itsuro Kato - katoitsu@dent.osaka-u.ac.jp; Soichi Iwai - s-iwai@dent.osaka-u.ac.jp; Koji Ono - onokoji@rri.kyoto-u.ac.jp; Minoru Suzuki - msuzuki@rri.kyoto-u.ac.jp; Yoshinori Sakurai - ysakurai@rri.kyoto-u.ac.jp; Ken Ohnishi - Kohnishi@naramed-u.ac.jp; Takeo Ohnishi - Tohnishi@naramed-u.ac.jp; Yoshiaki Yura* - yura@dent.osaka-u.ac.jp

* Corresponding author

Published: 11 December 2009

Radiation Oncology 2009, 4:63 doi:10.1186/1748-717X-4-63

Received: 3 September 2009
Accepted: 11 December 2009

This article is available from: http://www.ro-journal.com/content/4/1/63

Abstract

Background: Boron neutron capture therapy (BNCT) is a selective radiotherapy, being effective for the treatment of even advanced malignancies in head and neck regions as well as brain tumors and skin melanomas. To clarify the role of p53 gene, the effect of BNCT on oral squamous cell carcinoma (SCC) cells showing either wild- (SAS/neo) or mutant-type (SAS/mp53) p53 was examined.

Methods: Cells were exposed to neutron beams in the presence of boronophenylalanine (BPA) at Kyoto University Research Reactor. Treated cells were monitored for modulations in colony formation, proliferation, cell cycle, and expression of cell cycle-associated proteins.

Results: When SAS/neo and SAS/mp53 cells were subjected to BNCT, more suppressive effects on colony formation and cell viability were observed in SAS/neo compared with SAS/mp53 cells. Cell cycle arrest at the G1 checkpoint was observed in SAS/neo, but not in SAS/mp53. Apoptotic cells increased from 6 h after BNCT in SAS/neo and 48 h in SAS/mp53 cells. The expression of p21 was induced in SAS/neo only, but G2 arrest-associated proteins including Wee1, cdc2, and cyclin B1 were altered in both cell lines.

Conclusion: These results indicate that oral SCC cells with mutant-type are more resistant to BNCT than those with wild-type p53, and that the lack of G1 arrest and related apoptosis may contribute to the resistance. At a physical dose affecting the cell cycle, BNCT inhibits oral SCC cells in p53-dependent and -independent manners.

Background

Oral squamous cell carcinoma (SCC) patients are generally treated with surgery in combination with radiation therapy and/or chemotherapy [1,2].

Ionizing radiation (IR) directly damages DNA by causing single- and double-stranded breaks. p53 is a central mediator of the response to DNA damage and cell stress, therefore, it is expected to play a role in determining the

sensitivity of tumors to apoptotic stimuli such as radiation or cytotoxic drugs [3-6].

Boron neutron capture therapy (BNCT) is a binary modality: Boron-10 (^{10}B)-enriched compounds such as boronophenylalanine (BPA) and borocaptate sodium are administered at first, followed by irradiation with thermal neutrons. ^{10}B to captures thermal neutrons leads to the nuclear reaction ^{10}B (n, α) ^{7}Li. Both released particles, an α (^{4}He) particle and lithium (^{7}Li) nucleus have high linear energy transfer (LET) properties and short path lengths in water of 5-10 μm. If the boronated compounds selectively accumulate in the tumor, BNCT can be used to selectively destroy tumor cells [7,8]. It has been shown that BNCT is effective for the treatment of advanced malignancies in head and neck regions as well as brain tumors and skin melanomas [9-12].

The level of localized DNA damage caused by IR is believed to increase with elevating LET values of radiation. Cell inactivation induced by IR with different LET's has been analyzed, and many studies have shown that high LET radiation including carbon-ion beams is more effective than low LET X-rays and gamma rays regarding the yield of apoptosis and reproductive death [13-16]. Carbon-ion beams have been reported to increase apoptosis in oral SCC and lung cancer cells regardless of the p53 status [17,18].

Approximately 50% of oral SCCs show a mutational change of p53 [19,20]. Before the novel high LET radiation therapy BNCT is used more frequently for oral SCC, its effect on the cell cycle and the cytotoxic effect on oral SCC cells irrespective of the p53 status should be clarified. In the present study, we examined the effects of BNCT on the proliferation, cell cycle, and cell cycle-related proteins of oral SCC cells showing wild- or mutant-type p53 with the same background and indicated the role of p53 in the suppressive effect of BNCT.

Methods

Cells

The oral SCC cell line SAS showed the phenotype of wild-type p53 on IR-induced signal transduction. SAS cells were transfected with the plasmid pC53-248 containing an mp53 gene (codon 248, from Arg to Trp) to produce a dominant negative mp53 protein, or with the control plasmid pCMV-Neo-Bam, which contains a neo-resistance marker. The stable transfectants SAS/mp53 and SAS/neo were used [21]. These oral SCC cell lines were cultured in Dulbecco's modified Eagle's medium supplemented with 10% fetal bovine serum, 2 mM L-glutamine, 100 μg/ml penicillin, and 100 mg/ml streptomycin at 37°C in a humidified atmosphere with 5% CO_2.

Boron compound and BNCT for cultured cells

^{10}B-enriched (>98%) BPA was obtained from Boron Biologicals, Inc., (Raleigh, NC) and converted to a fructose complex following the method by Coderre et al. [22]. The concentration of the aqueous suspension of BPA was 250 mg/ml (21.28 mg ^{10}B/ml).

For BNCT, cells were grown in flasks with a culture area of 25 cm^2 and treated with BPA at a ^{10}B concentration of 50 ppm for 2 h. They were exposed to neutron beams in the presence of BPA at Kyoto University Research Reactor. Neutron fluence was measured by the radioactivation of gold foils on the front and back of the dishes, as described in previous studies [23,24]. The average fluence of thermal neutrons was 2.1×10^{12} n/cm^2, and the average flux was 2.3×10^{9} n/cm^2/s at 5 MW. Thermoluminescent dosimeters were used for gamma-ray dosimetry, and the total gamma ray dose was 0.00665 Gy. Thermal neutron fluence was converted to a dose, as described previously [24].

Colony formation assay

Colony formation was performed as described previously [24]. Briefly, cells were dissociated with 0.05% trypsin and 0.02% EDTA, suspended in medium, and plated onto 60-mm dishes at a cell density yielding approximately 500 colonies per dish. The cells were cultured for 7 days, fixed in methanol, and stained with 1% crystal violet. Colonies composed of more than 30 cells were counted. The surviving cell fraction was determined by dividing the colony number of the treated culture by that of the non-irradiated control culture.

3-(4, 5-dimethylthiazol-2-yl)-2,5-diphenyltetrazolium bromide (MTT) assay

MTT assay was performed following the method by Mosmann [25]. Cells were seeded in 96-well plates at a density of 1×10^3 cells/well. At various intervals after BNCT, 10 μl of 5 mg/ml MTT solution was added to each well with 100 μl of medium, and cells were incubated at 37°C for 4 h. After the addition of 100 μl of 0.04 N HCl in isopropanol, the plates were mixed thoroughly to dissolve the dark blue crystals. The plates were read on a Benchmark Plus microplate spectrophotometer (Bio-Rad Laboratories, Hercules, CA) with a reference wavelength of 630 nm and a test wavelength of 570 nm. Background absorbance at 630 nm was subtracted from the 570 nm reading. The values for BNCT-treated cells were calculated as a ratio in relation to the untreated control cells. Data are presented as the means ± SD of six determinations.

Flow cytometric analysis

Cells were dissociated and centrifuged, and the pellets were fixed in ice-cold 70% ethanol at -20°C overnight. Thereafter, the cells were washed twice with ice-cold PBS

and treated with 1 mg/ml RNase at 37°C for 30 min. After staining of cellular DNA with 50 μg/ml propidium iodide in PBS, cells were analyzed with a fluorescence-activated cell sorter (FACSort; Becton Dickinson, Mountain View, CA). The percentage of cells at different phases of the cell cycle was determined by employing Mod Fit LT software (Verity Software House, Topsham, ME). Based on an analysis of DNA histograms, the percentages of cells in sub-G1, G0/G1, S, and G2/M phases were evaluated.

Hoechst staining

Cells were dissociated and fixed in PBS containing 1% glutaraldehyde for 2 h. After washing in PBS, cells were stained with 200 μM Hoechst 33342, mounted on slides, and visualized using a Nikon Microphot-FXA fluorescence microscope. The number of positive cells was counted in 3 samples, and the mean ± SD was determined.

Immunoblot analysis

Cells were lysed in a buffer containing 20 mM Tris-HCl (pH 7.4), 0.1% sodium dodecyl sulfate, 1% TritonX-100, 1% sodium deoxycholate, and protease inhibitor cocktail. After sonication, cells were centrifuged at 15,000 × g for 10 min at 4°C, and the supernatant was harvested. Protein (20 μg) was separated through polyacrylamide gel electrophoresis and transferred to a polyvinylidene fluoride membrane by electroblotting. The membrane was probed with antibodies, and antibody-binding was detected using an enhanced chemiluminescence kit (Amersham Life Science, Arlington Heights, IL) according to the manufacturer's instructions. The antibodies used were as follows: mouse monoclonal antibodies against p53, p53 phosphorylated at serine-15, p21, cyclin B1, and β-actin, and rabbit polyclonal antibodies against Wee 1 and cdc2 phosphorylated at tyrosine -15. Antibodies against p53 and β-actin were obtained from Oncogene (San Diego, CA) and Sigma (St.Louis, MO), respectively. Those for Wee1 and cyclin B1 were from Upstate (Lake Placid, MA). Other antibodies were from Cell Signaling Technology (Beverly, MA). The β-actin expression was assessed to ensure protein loading.

Statistical analysis

The mean number of apoptotic cells was analyzed using the unpaired Student's *t*-test. A *P*- value < 0.05 was considered to be significant.

Results

Suppression of the colony formation of oral SCC cells by BNCT

SAS/neo and SAS/mp53 cells were treated with BNCT, and the survival ratios were calculated based on colony formation. In both cell lines, the survival ratios decreased in a dose-dependent manner, but SAS/neo were suppressed more strongly than SAS/mp53 cells. At a dose of 6 Gy, the survival fractions of SAS/neo and SAS/mp53 cells were 8 and 36%, respectively (Figure 1).

Suppression of the proliferation of oral SCC cells by BNCT

To determine the effect of BNCT on the proliferation of cells, SAS/neo and SAS/mp53 cells were treated with BNCT at a dose of 6 Gy. After incubation for 6, 12, 24, and 48 h, cell viability was measured by employing the MTT assay. When the BNCT-treated cultures were compared with those of untreated controls, the percentage of viable cells was decreased in both cell lines. The rates of viable SAS/neo and SAS/mp53 at 48 h after BNCT were 72 and 86% of untreated controls, respectively (Figure 2), showing a significant difference ($P < 0.01$).

Induction of cell cycle arrest by BNCT

SAS/neo cells were treated with BNCT at a dose of 6 Gy and then subjected to flow cytometric analysis. Initially, the rate of SAS/neo cells in the G0/G1 phase was 30%, and it increased to 39% at 6 h after BNCT. At 12 h, it decreased to 6%, and cells in the G2/M phase were increased to 34%. Sub-G1 peaks, indicating apoptotic cells, appeared from 6 h after BNCT (Figure 3). In SAS/mp53 cells, however, there was no increase of G0/G1 phase cells at 6 h after BNCT; rather, they decreased slightly (Figure 3). At 12 h after BNCT, the proportion of cells in the G2/M phase was increased to 40%, indicating arrest at the G2/M checkpoint. A small sub-G1 population appeared at 48 h after BNCT.

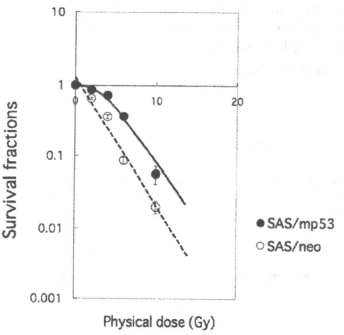

Figure 1
Suppression of the colony formation of oral SCC cells by BNCT. SAS/neo and SAS/mp53 cells were treated with BNCT, and survival fractions were assessed based on colony formation.

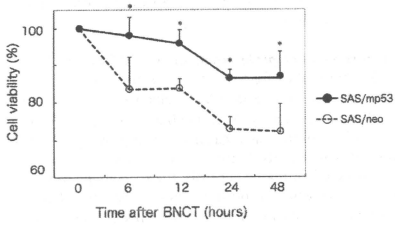

Figure 2
Suppression of the proliferation of oral SCC cells by BNCT. SAS/neo and SAS/mp53 cells were treated with BNCT, and cell viability was measured by the MTT assay. The cell viability of untreated cells was also measured and used as a control. *p < 0.01, SAS/neo vs. SAS/mp53.

Measurement of apoptotic cells by nuclear staining

Cell cycle analysis revealed the presence of a sub-G1 population, indicating apoptosis by BNCT. After treatment with BNCT, nuclear DNA was stained with Hoechst 33342, and cells showing nuclear fragmentation were determined (Figure 4A). In SAS/neo cells treated with BNCT, the proportion of apoptotic cells was elevated from 6 h as compared with untreated control cells, and reached 4.5% after incubation for 48 h (Figure 4B). The difference between SAS/neo and BNCT-treated SAS/neo was significant ($p < 0.01$). In the case of SAS/mp53, no apparent increase of apoptotic cells was observed early after BNCT, but the proportion increased to 3.5% at 48 h (Figure 4B). The difference between SAS/mp53 and BNCT-treated SAS/mp53 was significant ($p < 0.01$).

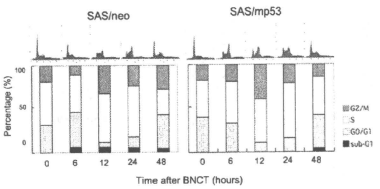

Figure 3
Induction of cell cycle arrest by BNCT. A. SAS/neo and SAS/mp53 cells were treated with BNCT and then subjected to flow cytometric analysis. **B.** Based on an analysis of DNA histograms, the percentages of cells in sub-G_1, G_0/G_1, S, and G_2/M phases were evaluated.

The expression and/or phosphorylation of G1 checkpoint-related proteins by BNCT

In BNCT-treated SAS/neo cells, the expression of p53 increased and reached its maximum 6 h after BNCT. The elevation of phosphorylated p53 was observed at 6, 24, and 48 h after BNCT. An increased expression of p21 was observed from 6 h after BNCT (Figure 5). In SAS/mp53, the protein level of p53 was not specifically altered, but the phosphorylation decreased gradually after BNCT. The expression of p21 was also suppressed after BNCT in SAS/mp53 cells.

The expression and/or phosphorylation of G2 checkpoint-related proteins by BNCT

In SAS/neo cells, the expression of Wee1 was elevated from 12 to 24 h after BNCT, and rapidly decreased at 48 h (Figure 6). The protein level of cdc2 increased from 12 h after BNCT, and this was maintained until 48 h. An increase in the phosphorylation of cdc2 occurred at 12 h, indicating cell cycle arrest at the G2 checkpoint, and declined to the initial level at 48 h. Cyclin B1 that forms the cdc2/cyclin B1 complex was induced at 12 h after BNCT. In SAS/mp53 cells, the expression of Wee1 increased at 12 and 24 h after BNCT (Figure 6). Although the protein level of cdc2 was not specifically altered, cdc2 phosphorylation increased at 12 h after BNCT. The protein level of cyclin B1 increased from 12 h after BNCT, and this was maintained until 48 h.

Discussion

It is considered that the presence of p53 mutation might reduce the effectiveness of radiotherapy, but studies comparing the presence or absence of p53 mutations in relation to the outcome following radiotherapy showed no consistent relationship [26-29]. Tumors with the wild-type p53 protein may lack a functional p53 response as a result of mutations affecting other genes that function in the same pathways as p53 [30]. It is difficult to clarify the role of p53 in each oral SCC cell line, and so we used known mutated oral SCC cell lines, SAS/neo and SAS/mp53, with the same background.

Studies on the correlation between the cytotoxic effect of BNCT and the p53 status are limited [31,32], but more studies are employing high LET carbon-ion beams. Indeed, Iwadate et al.[13] reported that high LET carbon-ion beams were more cytotoxic than low LET X-rays for glioma cells, and the effects of the carbon-ion beams were not dependent on the p53 gene status. Tsuboi et al. [15] reported that a glioblastoma cell line with p53 mutation was sensitive to carbon-ion beams as a wild-type p53 cell line at a high LET. In the present study, we performed colony formation assays, and confirmed that the effect of BNCT was more potent in SAS/neo than SAS/mp53 cells. We also examined the effect of BNCT using the MTT assay,

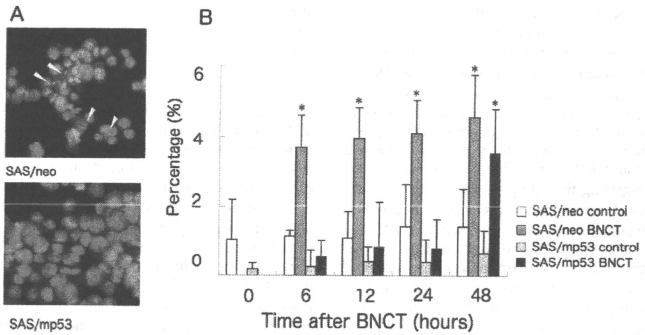

Figure 4
Induction of apoptotic cells with the fragmentation of nuclear DNA by BNCT. SAS/neo and SAS/mp53 cells were treated with BNCT, incubated for 48 h at 37°C, and stained by Hoechst 33342. The proportion of apoptotic cells was determined at various time points. *$p < 0.01$, SAS/neo vs. BNCT-treated SAS/neo; SAS/mp53 vs. BNCT-treated SAS/mp53.

and identified a difference between SAS/neo and SAS/mp53 cells regarding their proliferative potential after BNCT. The expression of functional p53 must be involved in BNCT-induced growth suppression and/or cell death.

p53 is a key factor that regulates the cell cycle checkpoint [4,6]. In this study, it was suggested that p53 plays an important role in G1 arrest in SAS/neo cells. Flow cytometric analysis revealed a transient accumulation in the G0/G population at 6 h after BNCT in SAS/neo cells. Thereafter, BNCT induced G2 arrest in both SAS/neo and SAS/mp53 cells. This indicates that BNCT induces cell cycle arrest at the G1 checkpoint only in SAS/neo cells. Tsuboi et al. [15] did not identify a marked increase of cells in the G1 phase in glioblastoma U87 MG cells with wild-type p53 as well as TK1 with mutant-type p53 after carbon-ion beam irradiation. BNCT may differ from carbon-ion beams in terms of its ability to induce cell cycle arrest at the G1 checkpoint.

When DNA damage by IR is irreparable, the activation of p53 leads to apoptosis via both transcription-dependent

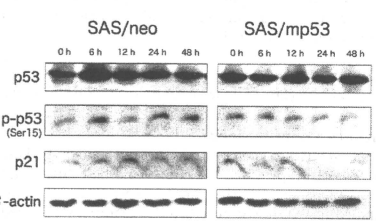

Figure 5
Altered expression and/or phosphorylation of G1 checkpoint-related proteins by BNCT. SAS/neo and SAS/mp53 cells were treated with BNCT, and the expression of p53 and p21 and phosphorylation of p53 were examined by immunoblot analysis.

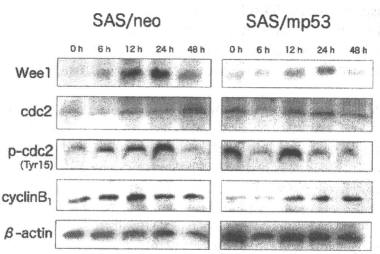

Figure 6
Altered expression and/or phosphorylation of G2 checkpoint-related proteins by BNCT. SAS/neo and SAS/mp53 cells were treated with BNCT, and the expression of Wee1, cdc2, and cyclin B1 and phosphorylation of cdc2 were examined by immunoblot analysis.